

# Active and Reactive Power Control of a Doubly Fed Induction Generator

Hung-Cheng Chen<sup>1,\*</sup> and Po-Hung Chen<sup>2</sup>

<sup>1</sup> Department of Electrical Engineering, National Chin-Yi University of Technology, 41107 Taichung City, Taiwan

<sup>2</sup> Department of Electrical Engineering, St. John's University, 25135 New Taipei City, Taiwan

Received: 21 Apr. 2013, Revised: 16 Aug. 2013, Accepted: 17 Aug. 2013

Published online: 1 Apr. 2014

**Abstract:** Doubly fed induction generators (DFIG) are increasingly used in grid interfaced wind energy systems to address voltage regulation and provide adequate reactive power support. This paper presents dynamic modeling and simulation of a doubly fed induction generator based on grid-side and rotor-side converter control. The DFIG, grid-side converter, rotor-side converter, and its controllers are performed in MATLAB/Simulink software. Dynamic response in grid connected mode for variable speed wind operation is investigated. Simulation results on a 3.6 MW DFIG system are provided to demonstrate the effectiveness of the proposed control strategy during variations of active and reactive power, rotor speed, and converter dc link voltage.

**Keywords:** Doubly Fed Induction Generator (DFIG), Grid-Side Converter, Rotor-Side Converter, Active and Reactive Power Control

## 1 Introduction

The wind power is a kind of renewable green power sources. It also is a permanent source without exploring and transporting. To solve the problem of energy's shortage and improve the environmental quality, wind power is used to produce electricity by a lot of countries [1,2]. The power output of a wind power plant is stochastic, which is determined by the wind speed and wind turbine generator. If a wind power plant consists of more wind turbine generators, the change of its power output will become drastic under wind speed fluctuation. With the development of wind industry, this kind of large wind power plants will bring many problems to the power system's operating [3,4,5]. Due to the quick development of power electronics and relative applications at present, the variable speed wind turbine with doubly fed induction generator (DFIG) was turned into mainstream machine in the field of exploiting wind energy in the world now [6,7]. Compared to wind turbines using fixed speed induction generators, DFIG-based wind turbines offer several advantages including four-quadrant active and reactive power capabilities, and variable speed operation. Such system also results in lower converter costs and lower power losses compared to a system based on a fully fed synchronous generator with full-rated converter [8,9,

10]. Therefore, the control technologies and the dynamic characteristics of the variable-speed constant-frequency (VSCF) doubly fed induction generator should be important topics in wind energy research [11,12,13]. In this paper, we study the dynamic characteristics of the DFIG and build the mathematical models accordingly. The complete MATLAB/Simulink model of a 3.6 MW DFIG generation system is built. Based on these models, dynamic response in grid connected mode for variable speed wind operation is investigated. From the analysis of the simulation results, we can realize that the DFIG active power output will keep varying with the change of the wind speed. The zero-reactive-power control in the ac-to-ac converter keeps the reactive power output near zero regardless of the wind speed fluctuation.

## 2 DFIG Modeling and Power Control

### 2.1 Generator Model

The classical governing equations of the DFIG in a  $d$ - $q$  synchronously rotating reference frame can be written as

\* Corresponding author e-mail: [hcchen@ncut.edu.tw](mailto:hcchen@ncut.edu.tw)

follows [14, 15]

$$\begin{aligned}
 v_{ds} &= -i_{ds}R_s + \frac{d\psi_{ds}}{dt} - \omega_1\psi_{qs} \\
 v_{qs} &= -i_{qs}R_s + \frac{d\psi_{qs}}{dt} + \omega_1\psi_{ds} \\
 v_{dr} &= i_{dr}R_r + \frac{d\psi_{dr}}{dt} - \omega_s\psi_{qr} \\
 v_{qr} &= i_{qr}R_r + \frac{d\psi_{qr}}{dt} + \omega_s\psi_{dr}
 \end{aligned} \quad (1)$$

The flux equations are

$$\begin{aligned}
 \psi_{ds} &= -L_s i_{ds} + L_m i_{dr} \\
 \psi_{qs} &= -L_s i_{qs} + L_m i_{qr} \\
 \psi_{dr} &= -L_r i_{dr} + L_m i_{ds} \\
 \psi_{qr} &= -L_r i_{qr} + L_m i_{qs}
 \end{aligned} \quad (2)$$

where

$\omega_1$ : synchronous angular frequency

$\omega_s$ : slip angular frequency

$R_s, R_r$ : equivalent resistances of stator and rotor windings, respectively

$L_s, L_r, L_m$ : self and mutual inductances of stator and rotor windings, respectively

The motion equations are given as follows

$$\begin{aligned}
 \frac{d\omega_r}{dt} &= (T_m - T_e)/J \\
 T_e &= \frac{3}{2}N_p L_m (i_{qs}i_{dr} - i_{ds}i_{qr}) \\
 \omega_s &= s\omega_1 = \omega_1 - \omega_r \\
 \frac{d\delta}{dt} &= \omega_r
 \end{aligned} \quad (3)$$

where

$\omega_r$ : rotor angular frequency

$s$ : slip

$T_m$ : mechanical torque provided to the wind turbine

$T_e$ : electromagnetic torque

$J$ : moment of inertia

## 2.2 Grid-Side Converter

The grid-side converter is a bi-directional AC/DC converter, which could work in rectifier state and inverter state. It is the major implementation elements of the DFIG slip power flow control [16, 17]. In order to study the three-phase PWM converter operation control, the model of PWM rectifier is derived as follows:

Figure 1 shows the AC equivalent diagram of the grid-side converter. The current flowing through the filter capacitor is

$$C \frac{dv_{dc}}{dt} = i_{dc} - i_L = S_a i_a + S_b i_b + S_c i_c - i_L \quad (4)$$

The voltage balance across the inductors is

$$\begin{bmatrix} v_a \\ v_b \\ v_c \end{bmatrix} = R \begin{bmatrix} i_a \\ i_b \\ i_c \end{bmatrix} + L \frac{d}{dt} \begin{bmatrix} i_a \\ i_b \\ i_c \end{bmatrix} + \begin{bmatrix} S_a \\ S_b \\ S_c \end{bmatrix} v_{dc} + \begin{bmatrix} u_n \\ u_n \\ u_n \end{bmatrix} \quad (5)$$

where

$S_a, S_b, S_c$ : three-phase bridge arm switching function, respectively.

$S = 1$ : the top switch is on and bottom is close

$S = 0$ : the bottom switch is on and top is close

$i_{dc}$ : DC link output current

$i_L$ : DC link load current

$v_{dc}$ : DC link output voltage

$C$ : filter capacitor

$L$ : inductance of grid-side reactor

$R$ : resistance of grid-side reactor

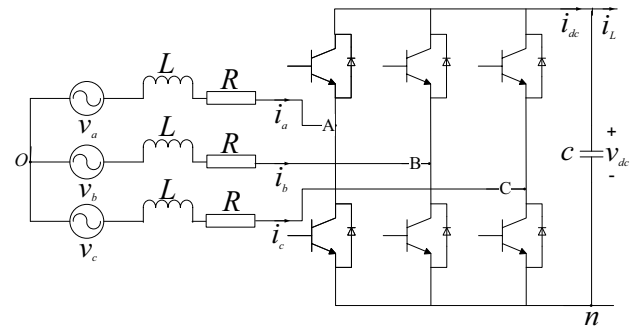


Fig. 1: Grid-side converter arrangement.

Due to the summation of the three-phase currents of the system without neutral line is zero, i.e.  $i_a + i_b + i_c = 0$ . We can obtain

$$u_n = \frac{v_a + v_b + v_c}{3} - \frac{1}{3}(S_a + S_b + S_c)v_{dc} \quad (6)$$

Defining  $i_d, i_q$  and  $v_{dc}$  as state variables and utilizing coordination transformation, the mathematical model of the three-phase converter in the two-phase rotating reference frame can be derived as

$$\begin{aligned}
 u_d &= -L \frac{di_d}{dt} - Ri_d + \omega_1 Li_q + v_d \\
 u_q &= -L \frac{di_q}{dt} - Ri_q - \omega_1 Li_d + v_q \\
 C \frac{d}{dt} v_{dc} &= i_{dc} - i_L
 \end{aligned} \quad (7)$$

where

$u_d, u_q$ : the  $d$ - $q$  components of bridge arm output voltage

$v_d, v_q$ : the  $d$ - $q$  components of grid voltage

$i_d, i_q$ : the  $d$ - $q$  components of input currents

Under the synchronously rotating frame, the  $d$  axis aligns with the grid voltage. The grid voltage components are

$$\begin{aligned} v_d &= \text{const} \\ v_q &= 0 \end{aligned} \quad (8)$$

Neglecting the harmonics due to switching in the converter and the machine losses or converter losses, the active power balance equation is

$$P_r = v_{dc}i_{dc} = \frac{3}{2}(v_d i_d + v_q i_q) = \frac{3}{2}v_d i_d \quad (9)$$

While  $P_r > 0$ , it represents grid-side converter works in rectifier state and absorbs energy from the grid. While  $P_r < 0$ , it represents grid-side converter works in inverter state and delivers energy to the grid from the DC side.

With the PWM depth  $m_1$  as known, we can relate  $v_d$  to  $v_{dc}$  as

$$v_d = \frac{m_1}{2\sqrt{2}}v_{dc} \quad (10)$$

From (9) and (10), the DC link output current and voltage can be derived as

$$i_{dc} = \frac{3m_1 i_d}{4\sqrt{2}} \quad (11)$$

and

$$C \frac{dv_{dc}}{dt} = i_{dc} - i_L = \frac{3m_1 i_d}{4\sqrt{2}} - i_L \quad (12)$$

It is evident from (12) that DC link voltage  $v_{dc}$  may be controlled through  $i_d$ . The reactive power  $Q_r$  from (to) the source is

$$Q_r = \frac{3}{2}(v_d i_q - v_q i_d) = \frac{3}{2}v_d i_q \quad (13)$$

According to the above equations, the reactive power to the grid-side converter from the source or to the source from the grid-side converter can be controlled through  $i_q$ . If the grid-side be controlled with a unit power factor, the  $i_q$  command value is equal to 0. For the sake of simplification, we assume two compensation terms  $u_{d1}$  and  $u_{q1}$  as

$$\begin{aligned} u_{d1} &= Ri_d + L \frac{di_d}{dt} \\ u_{q1} &= Ri_q + L \frac{di_q}{dt} \end{aligned} \quad (14)$$

Applying the above compensation terms to  $u_d$  and  $u_q$ , the effect of the cross-coupling of the input AC current can be eliminated. Furthermore, adding the feedforward compensation of the grid voltage, we can obtain the reference voltage  $u_d^*$  and  $u_q^*$

$$\begin{aligned} u_d^* &= -u_{d1} + (\omega_1 Li_q + v_d) \\ u_q^* &= -u_{q1} - (\omega_1 Li_d) \end{aligned} \quad (15)$$

The model of the vector control of the grid-side converter obtained from the above analysis is shown in Figure 2.

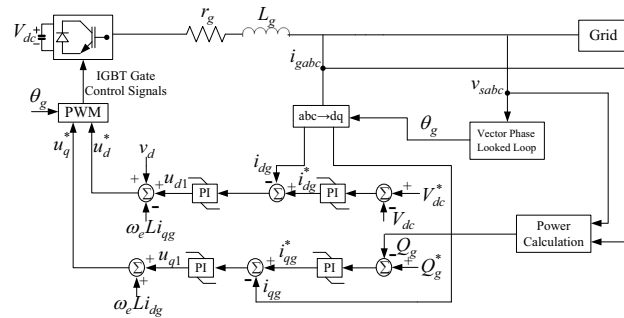


Fig. 2: Vector control model of the grid-side converter.

### 2.3 Rotor-Side Converter

Neglecting the resistance of the generator stator winding, the phase difference between stator flux and stator voltage vector is just  $90^\circ$ . Therefore, utilizing the stator flux-oriented to align the stator flux vector position with  $d$ -axis, the flux equation is

$$\begin{aligned} \psi_{ds} &= \psi_s \\ \psi_{qs} &= 0 \end{aligned} \quad (16)$$

To keep the stator flux  $\psi_s$  constant, the voltage equations can be expressed as

$$\begin{aligned} v_{ds} &\approx \frac{d}{dt} \psi_s = 0 \\ v_{qs} &\approx \omega_1 \psi_s = V_s \end{aligned} \quad (17)$$

where  $V_s$  is the space vector amplitude of stator voltage. The active and reactive powers of stator can be derived as

$$\begin{aligned} P_s &= \frac{3}{2}(v_{ds} i_{ds} + v_{qs} i_{qs}) \approx \frac{3}{2}V_s i_{qs} \\ Q_s &= \frac{3}{2}(v_{qs} i_{ds} - v_{ds} i_{qs}) \approx \frac{3}{2}V_s i_{ds} \end{aligned} \quad (18)$$

According to (18), while DFIG is connected to an infinite grid, the stator voltage is considered a constant. The stator current is the only controlled quantity. Therefore, the DFIG output power to grid can be controlled by the stator current, which achieves the goal of independent control for the DFIG active and reactive power output.

Due to the stator windings are directly connected to the power systems and the effect of the stator resistance is very small, the equivalent stator magnetizing current can be considered a constant, i.e.

$$i_{ms} = \frac{\psi_s}{L_m} \approx \frac{V_s}{L_m \omega_1} \quad (19)$$

Substituting equation (19) into equation (2),  $d$ - $q$  axis stator current can be calculated as

$$\begin{aligned} i_{ds} &= \frac{L_m i_{dr} - \psi_{ds}}{L_s} = \frac{L_m (i_{dr} - i_{ms})}{L_s} \\ i_{qs} &= \frac{L_m}{L_s} i_{qr} \end{aligned} \quad (20)$$

Substituting equation (20) into equation (1), the rotor voltage can be express as

$$\begin{aligned} v_{dr} &= i_{dr}R_r + \sigma L_r \frac{di_{dr}}{dt} - \omega_s \sigma L_r i_{qr} \\ v_{qr} &= i_{qr}R_r + \sigma L_r \frac{di_{qr}}{dt} + \omega_s \left( \sigma L_r i_{dr} + \frac{L_m^2}{L_s} i_{ms} \right) \end{aligned} \quad (21)$$

where  $\sigma = 1 - \frac{L_m^2}{L_s L_r}$  is the leakage factor.

The control variables  $v_{dr}$  and  $v_{qr}$  of the rotor voltage can be obtained from equation (21). The influence of the cross-coupling between the  $d$ - $q$  axis components of rotor current on system performance is small, which can be eliminated by adopting some control law. The model of the vector control of the rotor-side converter obtained from the above analysis is shown in Figure 3.

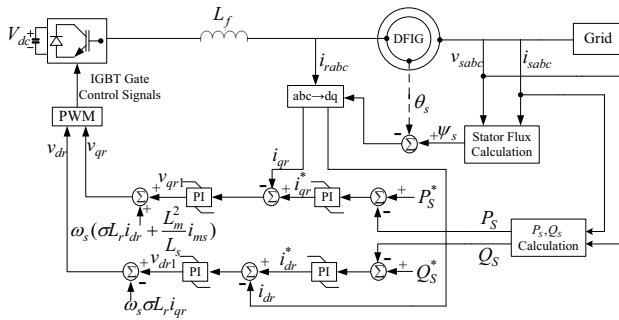


Fig. 3: Vector control model of the rotor-side converter.

### 3 Wind Speed Modeling

We utilized mathematical formulas to describe the variation of the wind speed, and built three different wind speed models. These models are detailed described in the following:

#### 3.1 Fitful Wind

The mathematical formula to build the model of the fitful wind is described as equation (22). In this work, the base wind velocity is 15m/s. The start-up time and variation cycle are 5s and 6s, respectively. The intensity of the fitful wind is 2m/s. The speed variation of the fitful wind is shown in Figure 4.

$$\begin{aligned} v_{WG} &= \begin{cases} 0, & t < t_{1G} \\ v_{COS}, & t_{1G} < t < t_{1G} + t_G \\ 0, & t > t_{1G} + t_G \end{cases} \\ v_{COS} &= \frac{MaxG}{2} \left[ 1 - \cos 2 \left( \frac{t}{t_G} - \frac{t_{1G}}{t_G} \right) \pi \right] \end{aligned} \quad (22)$$

where

- $t_{1G}$ : start-up time (s)
- $t_G$ : variation cycle (s)
- MaxG: intensity of fitful wind (m/s)

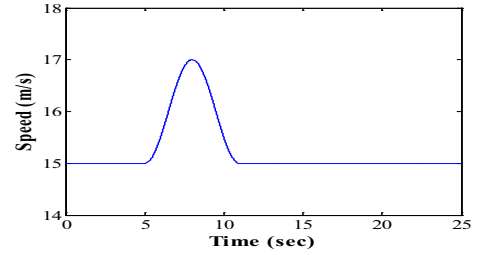


Fig. 4: Speed variation of fitful wind.

#### 3.2 Gradation Wind

The mathematical formula to build the model of the gradation wind is described as equation (23). The base wind velocity is 12m/s. The start-up time and stop time are 5s, 10s and 25s, respectively. The intensity of gradation wind is 4m/s. The speed variation of the fitful wind is shown in Figure 5.

$$\begin{aligned} v_{WR} &= \begin{cases} 0 & (t < t_{1R}) \\ v_{ramp} & (t_{1R} \leq t < t_{2R}) \\ MaxR & (t_{2R} \leq t < t_{2R} + t_R) \\ 0 & (t \geq t_{2R} + t_R) \end{cases} \\ v_{ramp} &= MaxR \left( 1 - \frac{t - t_{2R}}{t_{1R} - t_{2R}} \right) \end{aligned} \quad (23)$$

where

- $t_{1R}$ : start-up time (s)
- $t_{2R}$ : cut-off time (s)
- $t_R$ : stop time (s)
- MaxR: intensity of gradation wind (m/s)

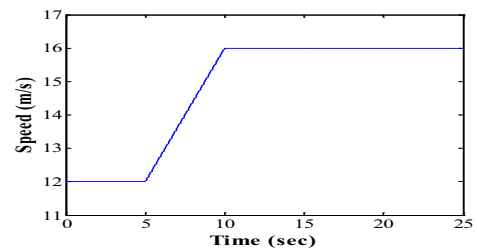


Fig. 5: Speed variation of gradation wind.

#### 3.3 Random Wind

The mathematical formula to build the model of the random wind is described as equation (24). The base

wind velocity is 15m/s. The intensity of random wind is 3m/s. The speed variation of the fitful wind is shown in Figure 6.

$$v_{WN} = v_N \text{Ran}(-1, 1) \cos(\omega_v t + \phi_v) \quad (24)$$

where

$v_N$ : intensity of random wind (m/s)

$\text{Ran}(-1, 1)$ : random sampling value (range between -1 to 1)

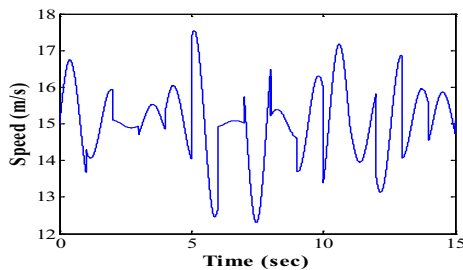


Fig. 6: Speed variation of random wind.

#### 4 Simulation Results and Discussion

The mathematical models of a 3.6 MW DFIG and its converters are derived. This system consists of a doubly fed induction generator with a four-quadrant ac-to-ac converter based on IGBTs connected to the rotor winding, and the stator winding directly connects to power systems. The rotor of the wind turbine is coupled to the generator shaft with a gear box.

The overall system structure of the DFIG-based wind generation system connected to a power system is shown in Figure 7. The output voltage of the DFIG is 4160V, which is increased to 22.8kV by a step-up transformer and connected to a power system through a 20km transmission line. The power system's rating voltage is 161kV which is dropped to 22.8kV by a step-down transformer. Based on these models, the effects of wind speed fluctuation on the operation characteristics of DFIG connected to a power system are studied by dynamic simulation.

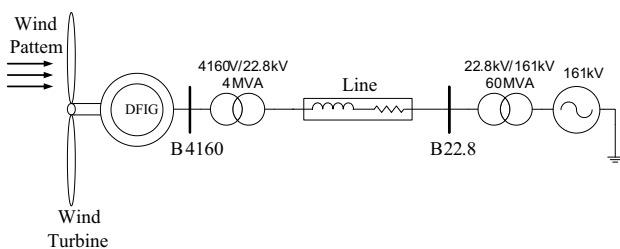
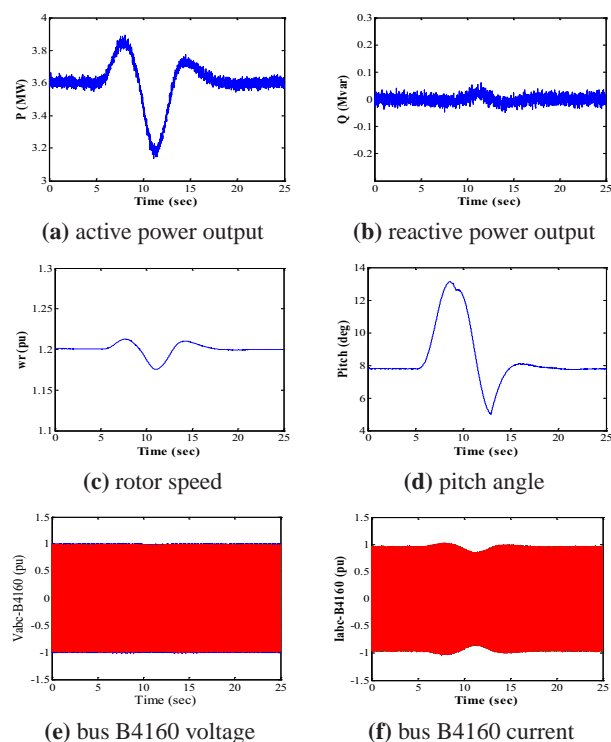
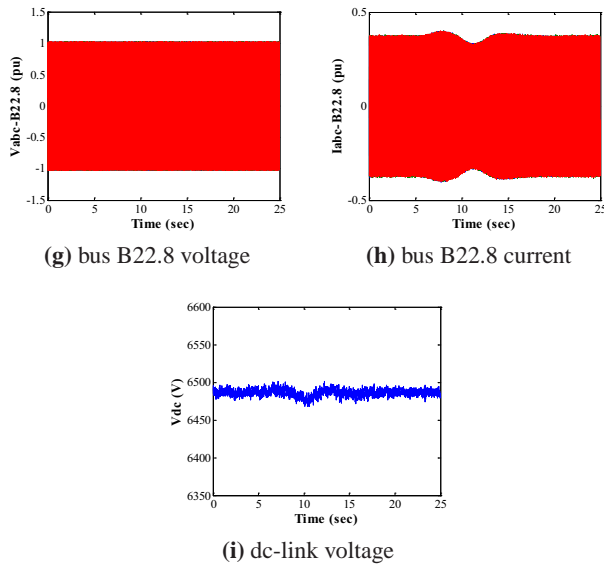


Fig. 7: Overall system structure of the DFIG-based wind generation system connected to a power system.

#### 4.1 Dynamic Responses of the DFIG under Fitful Wind Action

The dynamic responses of the DFIG generation system under a fitful wind action are shown in Figure 8. The active power output of the DFIG is shown in Figure 8(a). The wind speed arrives at maximum speed 17m/s at 8s at which the active power output increases to 3.85MW. Due to the temporary wind speed variation, the rotor speed shown in Figure 8(c) reduces after increasing and goes back to original speed 1.2pu because of the pitch angle of wind turbine adjusted accordingly. The variation of the active power output is therefore temporary and settles down at the original power output 3.6 MW. The controlled pitch angle of wind turbine to maintain constant power is shown in Figure 8(d). The pitch angle adjustment results in wind energy conversion under the maximum security. In Figure 8(b) the variation of the reactive power output followed the wind speed fluctuation is pretty small. The zero-reactive-power control in the ac-to-ac converter keeps the reactive power output near zero regardless of the wind speed fluctuation. The voltages at bus B4160 and B22.8 shown in Figure 8(e) and 8(g) maintain at 1pu. The currents at bus B4160 and B22.8 shown in Figure 8(f) and 8(h) vary with the wind speed fluctuation. The DC link voltage also varies with the wind speed fluctuation, but the variation is not obvious as shown in Figure 8(i). While the wind stops change all of the output variables eventually revert to original values.





**Fig. 8:** Dynamic responses of the DFIG under the fitful wind action.

### 4.2 Dynamic Responses of the DFIG under Gradation Wind Action

The speed variation of the gradation wind studied here linearly increase from 12m/s to 16m/s in 5 seconds. The dynamic responses of the DFIG generation system under the gradation wind action are shown in Figure 9. The original wind speed and active power output are 12m/s and 3.05MW, respectively. While the wind speed increases to 16m/s at 10s, the active power consequently increases to 3.95MW and then goes back to 3.6 MW because of the pitch angle adjustment as shown in Figure 9(d). The pitch angle approaches to 0 degree when the wind speed is below the rated wind speed (14m/s) of the DFIG to take advantage the wind energy by the optimal windward angle and generate the maximum output power. When the wind speed arrives at 16m/s, the pitch angle is adjusted to 10.5 degrees to keep the output power at rating and avoid an overload. The rotor speed also varies with the wind speed fluctuation. Although the wind speed has changed from 12m/s to 16m/s, the rotor speed shown in Figure 9(c) reduces after increasing and goes back to original speed 1.2pu because of the pitch angle control. The reactive power output is shown in Figure 9(b). The zero-reactive-power control in the ac-to-ac converter keeps the reactive power output near zero regardless of the wind speed fluctuation. The voltages at bus B4160 and B22.8 shown in Figure 9(e) and 9(g) maintain at 1pu. The currents at bus B4160 and B22.8 shown in Figure 9(f) and 9(h) vary with the wind speed fluctuation. The DC link voltage varies with the wind speed fluctuation, but the variation is not obvious as shown in Figure 9(i).

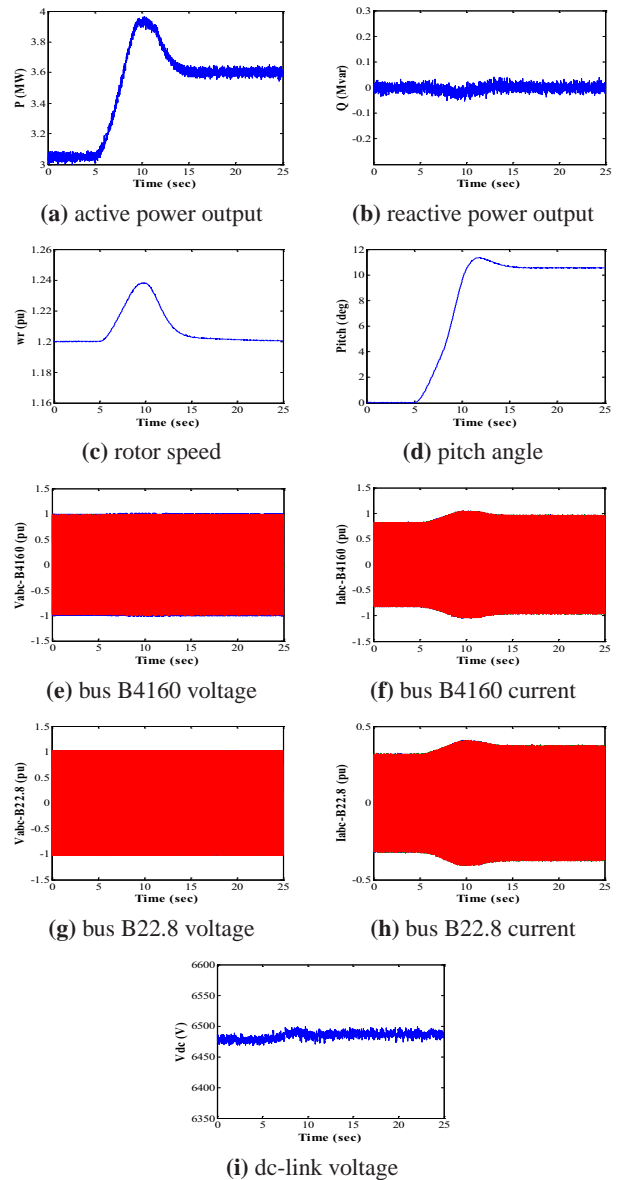


**Fig. 9:** Dynamic responses of the DFIG under the gradation wind action.

### 4.3 Dynamic Responses of the DFIG under Random Wind Action

The speed variation of the random wind studied here is shown in Figure 6, which randomly varies between 12.3m/s to 17.6m/s. The variations of active power, rotor speed, and pitch angle drastically vary with the wind speed change are shown in Figure 10(a), 10(c), and 10(d), respectively. The wind speed arrives at maximum speed 17.6m/s at 5s at which the active power output increases to 3.85MW. The rotor speed changes around to the original speed 1.2pu because of the pitch angle of wind turbine adjusted accordingly. The pitch angle adjustment

results in wind energy conversion under the maximum security. In Figure 10(b) the variation of the reactive power output followed the wind speed fluctuation is pretty small. However, the zero-reactive-power control in the ac-to-ac converter attempts to keep the reactive power output near zero under wind speed fluctuation. The voltages at bus B4160 and B22.8 shown in Figure 10(e) and 10(g) maintain at 1pu. The currents at bus B4160 and B22.8 shown in Figure 10(f) and 10(h) vary with the wind speed fluctuation. The DC link voltage varies with the wind speed fluctuation much obviously under the random wind action as shown in Figure 10(i).

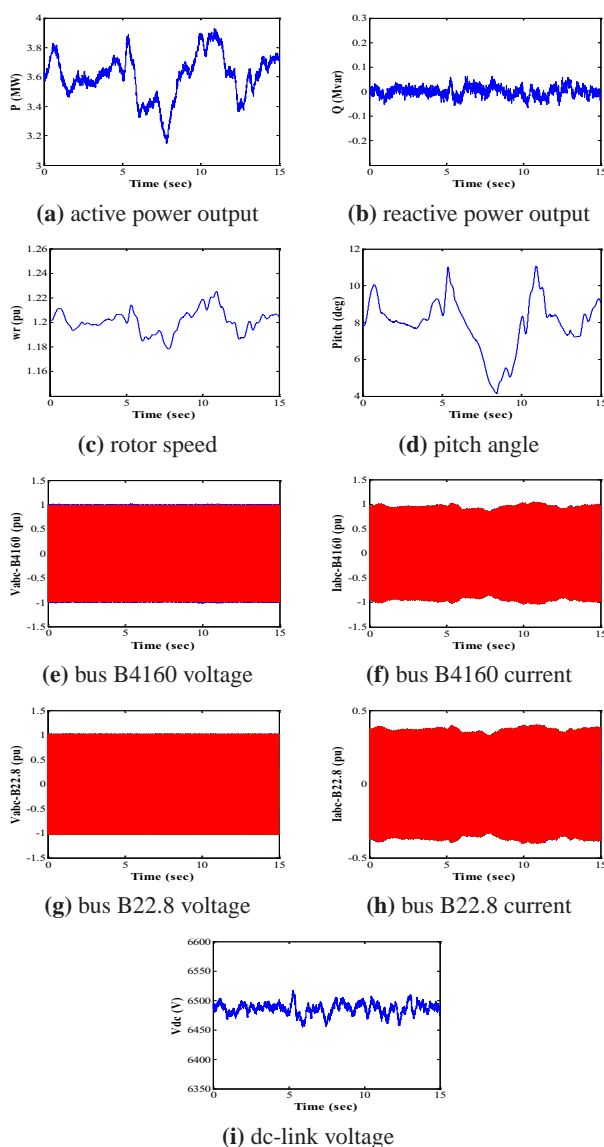


**Fig. 10:** Dynamic responses of the DFIG under the random wind action.

## 5 Conclusions

This paper studies the control of active and reactive power of the doubly fed induction generator connected to a power system. The direct control of the active and reactive power of the DFIG by the stator current provides global asymptotic regulation in presence of the stator current reference variation. Simulation results show that on active power in addition reactive power and consequently voltage maintain constant under variable wind speed operation.

## Acknowledgements

The support of this research by the National Science Council of the Republic of China (NSC) under Grants No. NSC-100-2623-E-167-001-ET and NSC-101-ET-E-167-003-ET is greatly appreciated.

## References

- [1] A. R. Ciupuliga, M. Gibescu, E. Pelgrum, P. G. H. Jacobs, K. P. J. Jansen, and W. L. Kling, Round-the-year security analysis with large-scale wind power integration, *IEEE Transactions on Sustainable Energy*, **3**, 85-93 (2012).
- [2] J. Liang, S. Grijalva, and R. G. Harley, Increased wind revenue and system security by trading wind power in energy and regulation reserve markets, *IEEE Transactions on Sustainable Energy*, **2**, 340-347 (2011).
- [3] H. Banakar, C. L. Luo, and B. T. Ooi, Impacts of wind power minute-to-minute variations on power system operation, *IEEE Transactions on Power Systems*, **23**, 150-160 (2008).
- [4] J. Kabouris and F. D. Kanellos, Impacts of large-scale wind penetration on designing and operation of electric power systems, *IEEE Transactions on Sustainable Energy*, **1**, 107-114 (2010).
- [5] Y. V. Makarov, P. V. Etingov, J. MA, Z. Y. Huang, and K. Subbarao, Incorporating uncertainty of wind power generation forecast into power system operation, dispatch, and unit commitment procedures, *IEEE Transactions on Sustainable Energy*, **2**, 433-442 (2010).
- [6] S. Muller, M. Deicke, W. Rik, and D. Doncher, Doubly fed induction generator system for wind turbines, *IEEE Industry Application Magazine*, **8**, 26-32 (2002).
- [7] R. Pena, J. Clare, and G. Asher, Doubly fed induction generator using back-to-back PWM converters and its application to variable-speed wind energy generation, *IEEE Proceedings, Electric Power Applications*, **143**, 231-241 (1996).
- [8] V. T. Phan and H. H. Lee, Performance enhancement of stand-alone DFIG systems with control of rotor and load side converters using resonant controllers, *IEEE Transactions on Industry Applications*, **48**, 199-210 (2012).
- [9] M. I. Martinez, G. Tapia, A. Susperregui, and H. Camblong, DFIG power generation capability and feasibility regions under unbalanced grid voltage conditions, *IEEE Transactions on Energy Conversion*, **26**, 1051-1062 (2011).

- [10] S. Muller, Adjustable speed generator for wind turbines based on doubly-fed induction machines and 4-quadrant IGBT converter linked to the rotor, In Proc. of the 2000 IEEE International Conference on Industry Applications, **4**, 2249-2254 (2000).
- [11] L. Qu and W. Qiao, Constant power control of DFIG wind turbines with supercapacitor energy storage, IEEE Transactions on Industry Applications, **47**, 359-367 (2011).
- [12] J. Hu, H. Nian, B. Hu, Y. He, and Z. Q. Zhu, Direct active and reactive power regulation of DFIG using sliding-mode control approach, IEEE Transactions on Energy Conversion, **25**, 1028-1039 (2010).
- [13] D. Y. Chwa and K. B. Lee, Variable structure control of the active and reactive powers for a DFIG in wind turbines, IEEE Transactions on Industry Applications, **46**, 2545-2555 (2010).
- [14] L. Xu and Y. Wang, Dynamic modeling and control of DFIG-based wind turbines under unbalanced network conditions, IEEE Transactions on Power Systems, **22**, 314-323 (2007).
- [15] A. Tapia, G. Tapia, J. X. Ostioza, and J. R. Saenz, Modeling and control of a wind turbine driven doubly fed induction generator, IEEE Transactions on Energy Conversion, **18**, 194-204 (2003).
- [16] L. Mihet-Popa, F. Blaabjerg, and I. Boldea, Wind turbine generator modeling and simulation where rotational speed is the controlled variable, IEEE Transactions on Industry Applications, **40**, 3-10 (2004).
- [17] L. Xu, Coordinated control of DFIG's rotor and grid side converters during network unbalance, IEEE Transactions on Power Electronics, **23**, 1041-1049 (2008).



**Hung-Cheng Chen** received both the M. S. and Ph.D. degrees in Electrical Engineering from National Taiwan University of Science and Technology in 1989 and 1993, respectively. He is currently an Associate Professor in the Department of Electrical Engineering, National Chin-Yi University of Technology, Taiwan. His research interests include renewable energy systems, micro grid control, and partial discharge diagnosis. Dr. Chen is a member of the IEEE Taipei Section.



**Po-Hung Chen** was born on April 21, 1963, in Taipei, Taiwan. He received the B.S. degree from the National Taiwan University of Science and Technology (NTUST), Taipei, the M.S. degree from the National Tsing Hua University, Hsinchu, Taiwan, and the Ph.D. degree from the NTUST, in 1986, 1989, and 1997, respectively, all in electrical engineering. Since 1989, he has been with the St. John's University, Taipei, where he is currently an Associate Professor in the Department of Electrical Engineering. His current research interests include power system planning, partial discharge measurement, and renewable generation techniques. Dr. Chen is a member of the IEEE Taipei Section.